INFORMATION TO USERS

This manuscript has been reproduced from the microfilm master. UMI films the text directly from the original or copy submitted. Thus, some thesis and dissertation copies are in typewriter face, while others may be from any type of computer printer.

The quality of this reproduction is dependent upon the quality of the copy submitted. Broken or indistinct print, colored or poor quality illustrations and photographs, print bleedthrough, substandard margins, and improper alignment can adversely affect reproduction.

In the unlikely event that the author did not send UMI a complete manuscript and there are missing pages, these will be noted. Also, if unauthorized copyright material had to be removed, a note will indicate the deletion.

Oversize materials (e.g., maps, drawings, charts) are reproduced by sectioning the original, beginning at the upper left-hand corner and continuing from left to right in equal sections with small overlaps. Each original is also photographed in one exposure and is included in reduced form at the back of the book.

Photographs included in the original manuscript have been reproduced xerographically in this copy. Higher quality 6" x 9" black and white photographic prints are available for any photographs or illustrations appearing in this copy for an additional charge. Contact UMI directly to order.

UMI

A Bell & Howell Information Company
300 North Zeeb Road, Ann Arbor MI 48106-1346 USA
313/761-4700 800/521-0600

Université d'Ottawa · University of Ottawa

Ion-Surface Scattering Measurements of the (110) Surface of TiO_2

by Jennifer A. Seel

Thesis submitted to the School of Graduate Studies
and Research in partial fulfillment of the requirements
for the Master of Science degree in Physics.

Physics Department
Faculty of Science
University of Ottawa
Ottawa, Canada

Abstract

The (110) surface of TiO_2 is examined using a 9.92 keV oxygen ion beam. The positions of the peaks in the emitted ion energy spectrum are consistent with those predicted by ion-surface scattering theory for O^+-O and O^+-Ti collisions. Upon examination of the peaks present in the ion energy spectrum, information about the surface crystallographic structure can be determined. This includes studying the shadowing/blocking effects as the azimuthal and elevation angles are varied. Using this information the dimensions of the surface unit cell are found to be consistent with the bulk dimensions. The height of the oxygen rows that are present above the surface can also be determined and is found to be lower than predicted by the bulk.

Acknowledgments

I would like to express my thanks to Dr. Brain Hird for accepting to do my MSc degree with him and I would like to thank him for many helpful discussions and patience he showed me throughout my degree.

I would also like to that Dr. Robert A. Armstrong for his helpful discussions and help with the programming and to Bruno Riel and Dr. Peter Piercy for their helpful discussions.

I also extend my thanks to the members of both the machine shop for their prompt construction of new apparatus and to the members of the electronics shop for their help with circuits and computer problems.

Table of Contents

List of Figures and Tables

Figures

Tables

Chapter 1 Introduction

Ion scattering techniques are a useful tool in obtaining information about the crystallographic structure and the atoms present on a surface. Since low energy ion scattering (LEIS) has a low range of energies, 1 to 20 keV, it allows an investigation into the first few atomic layers of the substrate which makes it a good technique for surface studies. This technique can also be used to study the scattering process, channeling, shadowing and blocking effects as well as neutralization processes [1-3]. The information obtained about a surface from LEIS studies compliments those done by Auger processes, scanning tunneling microscopy, STM, measurements and many others.

Generally, most ion-surface scattering (ISS) techniques erode the surface and the emitted atoms are identified using a mass spectrometer. By contrast, a specially designed LEIS was developed to minimize the surface damage during ion bombardment. The energies of the emitted particles are identified through the use of an energy analyzer. Not only the surface can be examined using LEIS but the scattering process itself can be investigated. The collisions between the incoming ions and the surface atoms can be treated classically with a reasonable degree of accuracy and results in a direct interpretation which allows identification of surface atoms and measurements of the relative positions of those atoms.

Other surface techniques such as low energy electron diffraction (LEED) and reflection high energy electron diffraction (RHEED) look at the long range order of the

sample whereas LEIS does not require long range order and primarily examines the relative positions of nearby atoms. RHEED can give a rough approximation to the relative positions of the surface atoms as well as an idea of the surface roughness. This approximation is obtained indirectly since diffraction experiments measure properties of k space and not of real space as done in LEIS. Since this difference is present, RHEED will be used to obtain an idea of the smoothness of the surface and an estimate of the surface unit cell dimensions and will hence compliment any measurements obtained through LEIS.

Several studies of the surface of TiO_2 have been previously performed but these are mainly Auger and STM measurements as well as some LEED and MEED studies (medium energy electron diffraction) [4-10]. Very few ion scattering measurements have been done in comparison [3,11,12]. Because of this the dimensions of the unit cell obtained by LEIS can be compared to measurements already obtained by other methods as well as possibly providing new information about the surface.

The exact structure of the surface still remains to be completely determined. The main purpose of this work is to obtain as much information about the surface structure of TiO_2 as possible. More specifically, to confirm the dimensions of the surface unit cell and to obtain an estimate of the height of the oxygen rows which are present on the surface.

Chapter 2 Theoretical and Other Considerations

2.1 Binary Collisions

The binary collision model has been found to give a reasonable description of the interaction between an ion and an atom on the surface of a solid [13, 14]. This model is valid if the following assumptions are made: the atoms in the surface region are unbound to its neighbours, i.e. the other atoms on the surface will not affect the collision; the target atom is stationary; and the energy losses are kinetic. The first assumption is valid since the kinetic energy of the incident ion is much greater than the binding energy of the target atoms. The second is valid since most vibrational energies are about 0.04 eV, at room temperature, which is quite small in comparison with the energy of the incident ion. The losses that are due to inelastic effects such as electronic excitation or ionization are usually small enough to have no affect within the energy resolution of the experiment. If any of the effects stated above are considered or if the possibility of multiple collisions with more than one atom are considered, the model would be more accurate but this simple binary collision model has been shown to be sufficient.

For simple two body elastic scattering the energies of the scattered (E_s) and recoiled (E_r) ions/atoms can be calculated from the conservation of momentum and energy and are dependent on the scattering angle, θ, or the recoil angle, ϕ, and the ratio, A, of the target mass, m_2, and the incident ion mass, m_1, so that $A = m_2/m_1$.

$$k_s = \frac{E_s}{E_o} = \left(\frac{\cos\theta \pm \left(A^2 - \sin^2\theta\right)^{1/2}}{1+A} \right)^2 \qquad (1)$$

$$k_r = \frac{E_r}{E_o} = \frac{4A(\cos\phi)^2}{(1+A)^2} \qquad (2)$$

where E_o is the incident ion energy. The angles involved can be seen pictorially in Figure 2.1. Experimentally, for ions of a few keV, peaks in the scattered ion spectrum are observed which fit well with these relations and so can be associated with single binary collisions with surface atoms. The peaks have finite width, due to more complicated processes but the maximum usually occurs at an energy ratio close to that predicted by equations (1) and (2).

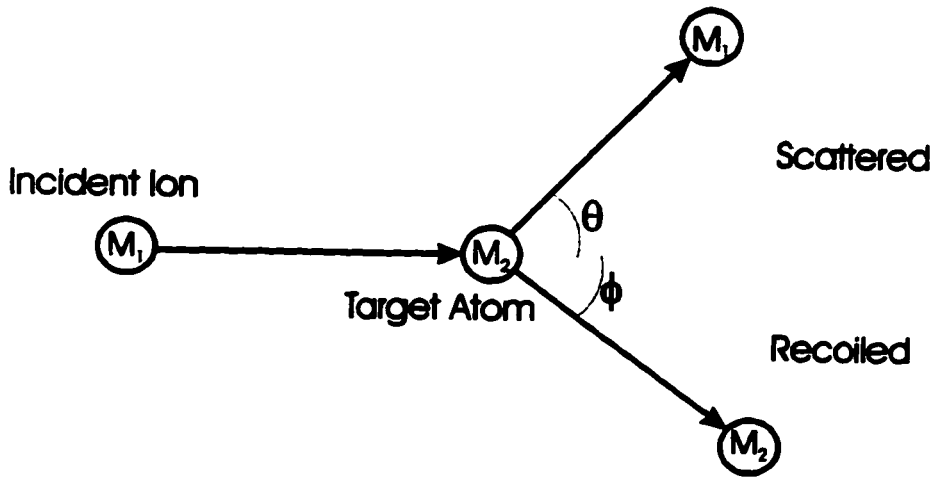

Figure 2.1 Angles involved in the single collision

There are two different cases possible in equation (1) which depend on the relative masses of the two particles involved in the collision. If $m_1 \leq m_2$, i.e. $A \geq 1$, then to obtain a positive solution the plus sign must be used. If $A < 1$, both signs can be used as they both give positive energy ratios. When $A \leq \sin\theta$, two positive physical solutions exist

which represent two different processes at the same scattering angle.. However, the negative sign, which corresponds to backward center-of-mass scattering transformed to forward scattering in the lab frame, is usually much less intense and can usually be ignored in measurements. The dependence of k_s and k_r on their corresponding angles are shown for several values of A in Figure 2.2. Since backward recoil is impossible: $0 \leq \phi \leq 90°$. The range of θ depends on A; for $A < 1$: $0 \leq \theta \leq \sin^{-1}A$ but for $A > 1$: $0 \leq \theta \leq 180°$.

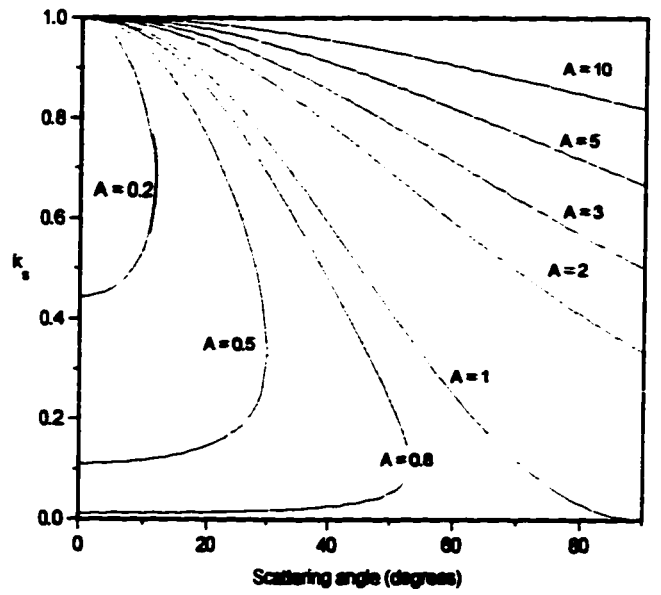

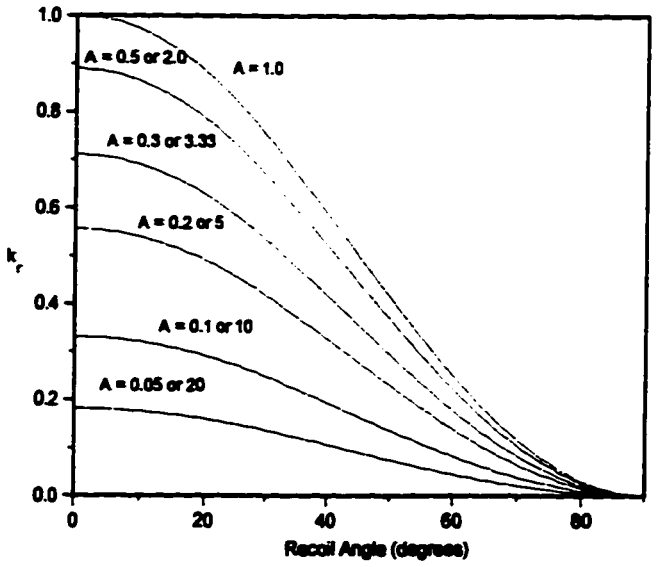

Figure 2.2 The fraction of scattered (k_s) and recoiled (k_r) energies for different mass ratios (A)

Though these predictions agree well with experimental results, the peaks often appear to have high energy shoulders and sometimes a peak may be very broad. These effects are due to multiple scattering; i.e., the incoming ion is deflected significantly by more than one atom but the total scattering angle is the same as for single scattering. Under these conditions the outgoing particle can have more energy than if there was only one collision. For example, consider an oxygen ion colliding with a titanium atom at a total scattering angle of 45°. With only one collision, the value of k_s would be 0.8202. If there were two collisions, one being 5° and the other being 40° would result in $k_s = k_{s1} * k_{s2}$ = 0.8518. The maximum scattered ion energy, for a given total scattering angle, occurs when each of the individual scattering angles are equal, i.e. when each scattering angle is θ/n for n collisions. For the example stated above the maximum k_s would be 0.9031. For a complete picture of this variation refer to Figure 2.3. In this figure the value of $k_{s1} * k_{s2}$ is given for two different total scattering angles and for two different set of collisions, one involving oxygen atoms and the other involving titanium and oxygen atoms.

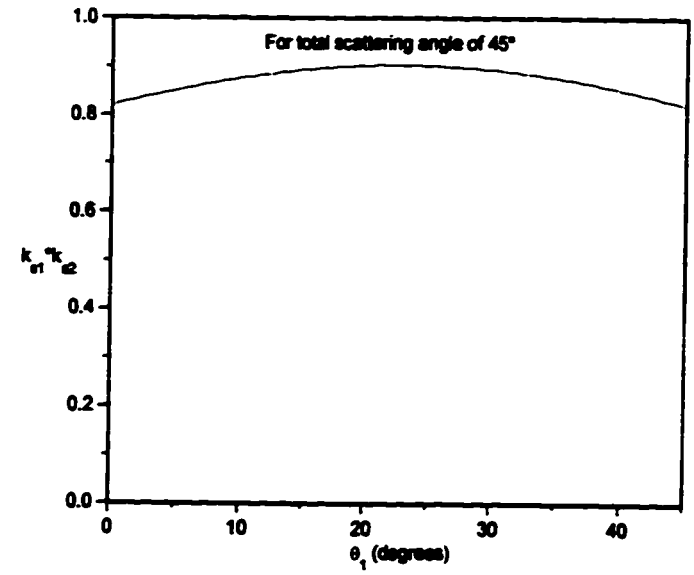

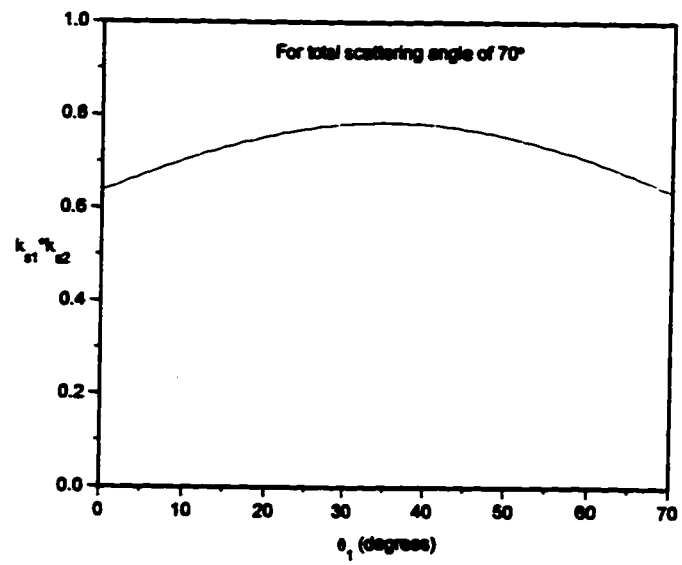

Figure 2.3 Illustration of $k_{s1}*k_{s2}$ for two possible angles and for two different collisions. The dashed lines represent a double collision involving oxygen atoms whereas the solid lines represent a double collision involved an oxygen and titanium atoms.

2.2 Shadowing effects

When an energetic ion collides with a surface atom it is deflected causing the incident ion's trajectory to be unaltered by atoms lying behind the struck atom in the direction of the ion beam. These atoms are said to be hidden by a shadow cone, see Figure 2.4.

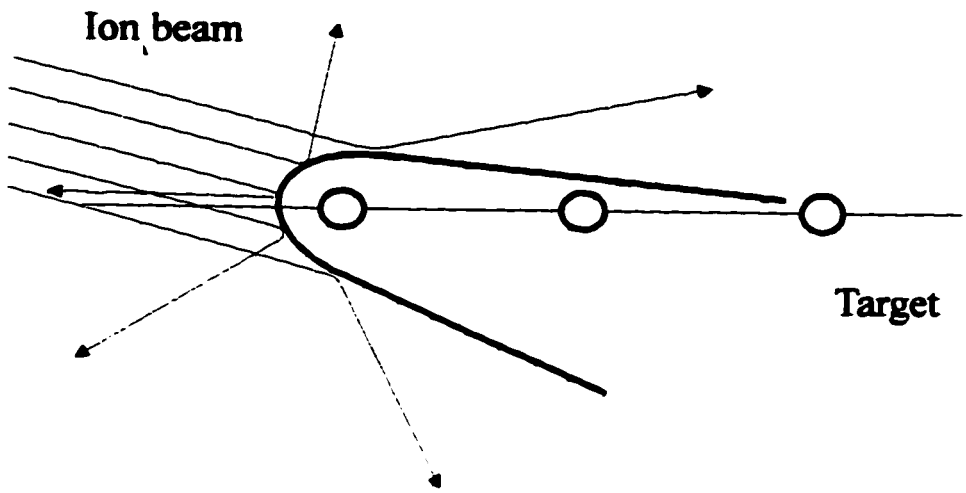

Figure 2. 4 A typical shadow cone

The shape of the shadow cone can be calculated from individual trajectories of the collision using many different impact parameters. As the impact parameter is increased the scattering decreases and the point at which neighbouring trajectories intersect can be used to define the locus of the shadow cone.

For any given impact parameter and ion energy the trajectories can be calculated using the classical equations of motion for a single moving particle and a fixed center of force or potential. The scattering angle in terms of a potential is

$$\theta = \pi - 2\int_{r_m}^{\infty} \frac{b\,dr}{r^2}\left(1 - \frac{V(r)}{E} - \frac{b^2}{r^2}\right)^{-1/2} \qquad (3)$$

where r is the interatomic distance, b is the impact parameter, E is the kinetic energy of the collision, V(r) is the potential and r_m is the value of r which gives zero for the quantity in the square root, which is the distance of closest approach [15-17]. To actually obtain a value for θ, it is necessary to assume some radial dependence for the central potential which is used to simulate the ion-atom interaction. For most forms of V(r), equation (3) must be solved numerically, though for some special potentials such as the Coulomb potential an analytic solution does exist. Two types of potentials that have been commonly used are inverse power potentials and purely exponential potentials. The most commonly used potential is the screened Coulomb (or Molière) potential which modifies the 1/r short range Coulomb potential with an exponential screening term.

$$V(r) = \frac{Z_1 Z_2 e^2}{r}\beta \exp(-\delta r/a) \qquad (4)$$

where Z_1 and Z_2 are the atomic number of the ion and target atom respectively, e is the electronic charge, a is the screening parameter, and β and δ are two more parameters. The values of a, β, and δ can be changed so that the trajectories and hence the shadow cone radius or angle fit experimental data. Presently, the potential that is used is a sum of three potentials of the form in equation (4), with six adjustable parameters, β_1, β_2, β_3, δ_1, δ_2 and δ_3 to fit a large body of experimental scattering data.

Knowledge of the shape of the shadow cone and shadow cone angle can be used to determine the relative positions of atoms on the surface. This is done by varying the angle at which the ion beam strikes the surface, θ_{in}. As θ_{in} is increased there will be a point at which many more surface atoms are seen. This is known as the critical angle and it corresponds roughly to the shadow cone angle. This process will be discussed in greater detail in section 4.5.

2.3 Structure of TiO_2

Titanium dioxide is very useful in such processes as photoelectrolysis, photo-assisted and photocatalytic reactions and also in photo-oxidation of organic molecules and H_2O. It would be extremely helpful to obtain a complete picture of the surface structure and properties, electrical, chemical and physical, of TiO_2 as this would help in the understanding of such reactions and processes.

There are three structural types of TiO_2. The most stable one and the one used in this work is referred to as having a rutile structure. The other two types of structure are anatase and brooklite. The rutile structure is tetragonal with a = b = 4.59Å and c = 2.96Å, see Figure 2.5 [4].

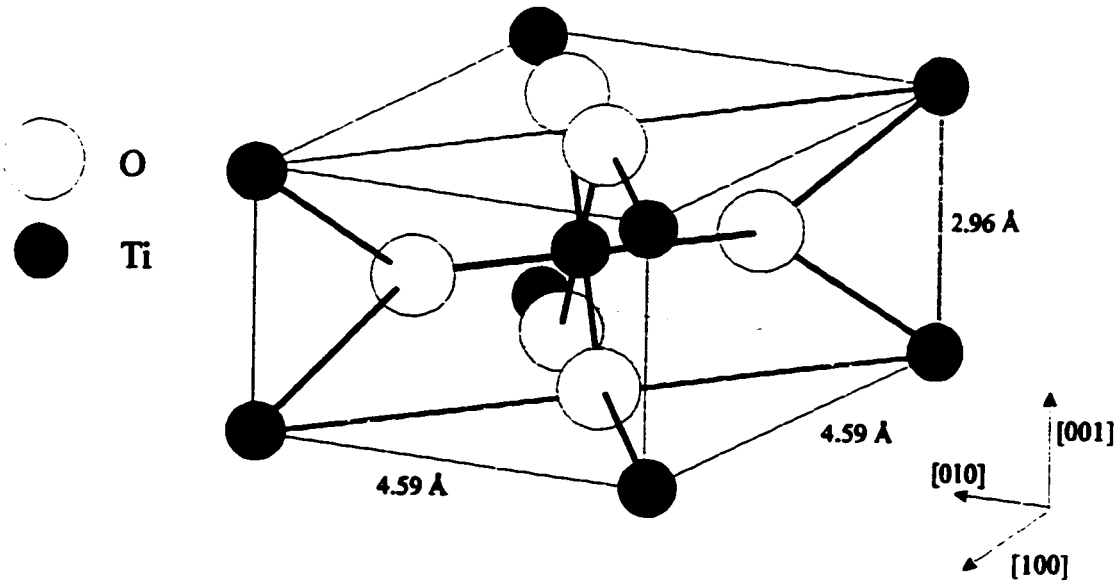

Figure 2.5 The unit cell of TiO_2 with a = b = 4.59Å and c = 2.96Å. The shaded plane is the (110) surface plane.

The valence band and conduction band of TiO_2 are due to O(2p) and Ti(3d) orbitals, respectively [4]. The optical band gap is approximately 3.0 eV at room temperature [4]. It is a partially ionic semiconductor and is used as a high dielectric material for thin film capacitors. The bulk resistivity of TiO_2 is 10^{11} Ωm. This value can be reduced considerably by electron beam bombardment to a value of about $5x10^{-4}$ Ωm [18].

There have been several studies of the (001), (100) and (110) surfaces. It was found that the (001) surface facets after annealing. According to Kurtz [19], if the annealing temperature is above (below) 1200K, (011) ((114)) facets will appear. However, Chung et al [4] have found that (100) and (110) facets appear and it is independent of the annealing temperature over the range of 673-1073K. Wang et al [20] has found that {214} planes will appear after annealing.

The (100) surface was found to be fairly stable if annealed in oxygen [20]. However, Kurtz [19] and Chung et al [4] found that the surface reconstructs to different structures depending on the annealing temperature. The possible reconstructions and temperatures are: (1x3) for 773-873K, (1x5) for 1073K, (1x7) for 1473K. Chung states that these reconstructions are all stable at room temperature and correspond to successively less oxygen on the surface.

The surface used in this work was the (110) surface which is the plane that cuts through the body diagonal of the unit cell. The widely accepted model for the surface is that it retains the bulk like structure with rows of oxygen atoms that lie above the main surface layer along the <001> direction, see Figure 2.6, bridging two titanium atoms [5].

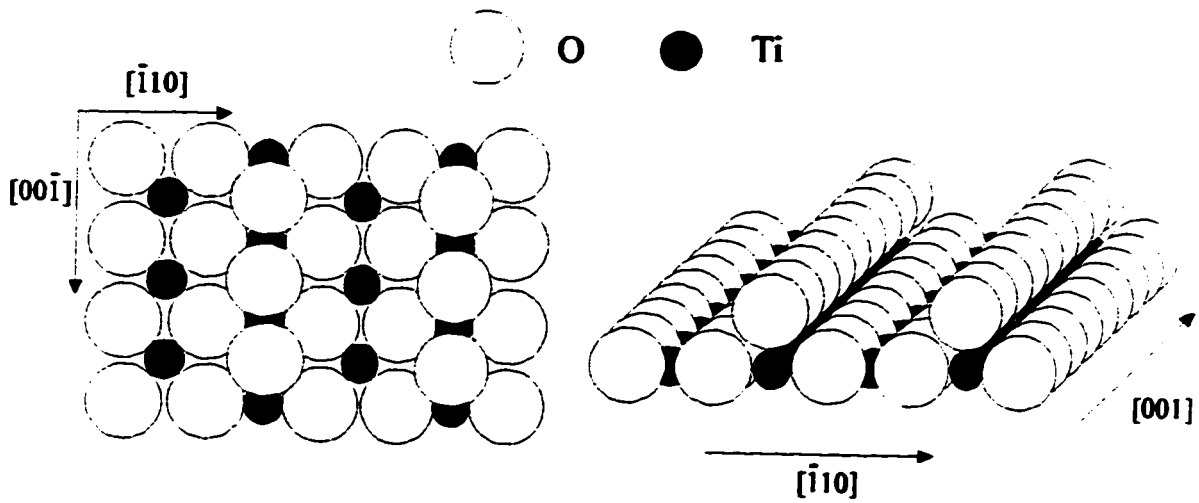

Figure 2.6 The details of the (110) surface.

There is much more information available on the (110) surface than the (001) and (100) surfaces but there is conflicting evidence as to whether the surface is stable, i.e. whether it will reconstruct or not. Early work has shown that the (110) surface was stable and did not reconstruct at least in the 873-1073K annealing temperature range[4, 6, 19, 21, 22]. Kao et al [21], however, using scanning tunneling microscopy (STM), found that the surface will reconstruct to a (1x2) structure if annealed to 900K. Other groups have since also produced this reconstruction. By using low energy electron defraction (LEED) and Auger electron microscopy (AES), Møller found that the (1x2) reconstruction occurred when the surface was heated to 823K (for about 3 hours) [23]. It is thought that this temperature is not sufficiently high to merge any steps and/or kinks on the surface. However, upon further annealing to 973K the surface a (1x1) structure appeared; i.e. the process is reversible. This disagrees with the results found by Hiroshi et al [24] who found, through the use of STM, that after annealing to 1150K the (1x2) structure

appeared and the (1x1) structure could not be restored through further annealing. They also found that steps and terraces were produced at lower annealing temperatures, 400-800K and 860K, respectively. Also by STM, Sander et al [7] found that if the (110) surface was heated to temperatures exceeding 973K , it would reconstruct to the (1x2) structure, however, if the (110) surface was annealed in oxygen, it did not reconstruct. Szabo et al [8] found, using STM, that the (1x1) structure is most stable when annealed at low temperature and will convert to a (1x2) structure when heated to temperatures exceeding 1000K. Møller [23] also showed that this (1x2) structure occurs because of the competition between the desorption of oxygen into the vacuum and diffusion of oxygen from the bulk to the surface. Also, previous work has shown that the surface structure is consistent with that of the bulk [9].

The amount of oxygen present on the surface and within the bulk of the sample changes as the sample is bombarded and exposed to various substances. Upon sputtering oxygen is removed from the surface. This deficiency of oxygen can be replenished by annealing in vacuum. During the anneal, oxygen desorbs from the surface into the vacuum and oxygen from within the bulk diffuses to the surface. The net result, i.e. the equilibrium state, is that oxygen diffuses to and therefore replenishes the surface. This diffusion causes the sample to change colour from a milky white or yellow to a dark blue and eventually to a metallic gray. If the sample is heated in oxygen the surface oxygen can be restored without depleting the bulk oxygen. If the sample is baked in a high enough pressure of oxygen, some of the depleted bulk oxygen may also be restored.

The most common impurities that are present in TiO_2 are S, Cl, K, C and Ca [4] but since these impurities are usually of such a low concentration they are easily removed by sputter cleaning (argon bombardment) and by annealing. Besides removing impurities, a stoichiometric surface is also desired before performing surface experiments. There is some disagreement on which cleaning procedure produces the best surface. Several groups have suggested that cycles of Ar sputter cleaning and annealing in UHV is the best procedure for their experiments, however the temperature of the anneal differs, ranging from 900K to 1200K, [6, 12, 24-26]. After several cycles some say that to obtain a stoichiometric surface one needs to then anneal in oxygen [6, 25] but others say this is not necessary [26]. Other groups only sputter and anneal through one cycle and again some say it is best to anneal in oxygen [7, 10] but others say in UHV [4, 22, 27] and still others say to first anneal in oxygen and then in UHV [9, 11]. The main concern of the groups that insist that a heat or anneal in oxygen is required is to replace the surface oxygen that is lost during sputtering without depleting the bulk. Depending on the type of experiment performed a stoichiometric bulk may not be necessary, as long as the first several layers of the sample are stoichiometric. These experiments suggest that after argon sputtering an anneal to about 900K or so, and possibly even an anneal in a low pressure of oxygen rather than in UHV is necessary to obtain a clean surface and to restore the surface stoichiometry.

Chapter 3 Experimental Setup and Preparation

3.1 Experimental Setup

There are three main sections to the ion-scattering experimental setup. These are: 1) the accelerator section; 2) the differential section; and 3) the main chamber (see Figure 3.1). The first two sections are required to create, select and collimate the beam; the actual experiment is performed in the main chamber. The production and mass selection processes have been unchanged from previous work [28] and will therefore be described briefly.

3.1.1 Accelerator Section

The beam is produced by a radio-frequency (RF) ion source. The ion beam is then accelerated to a high voltage followed by deceleration to the desired lower values, usually within the 2-10 kV range. After acceleration it is mass selected. This is done through the use of a 30° beam bending magnet. The magnet deflects ions of different masses at different radii of curvature which allows for easy separation of the ions. This mass scan is taken to identify the type of ions that pass through into the main chamber while varying the current through the magnet and hence varying the magnetic field.

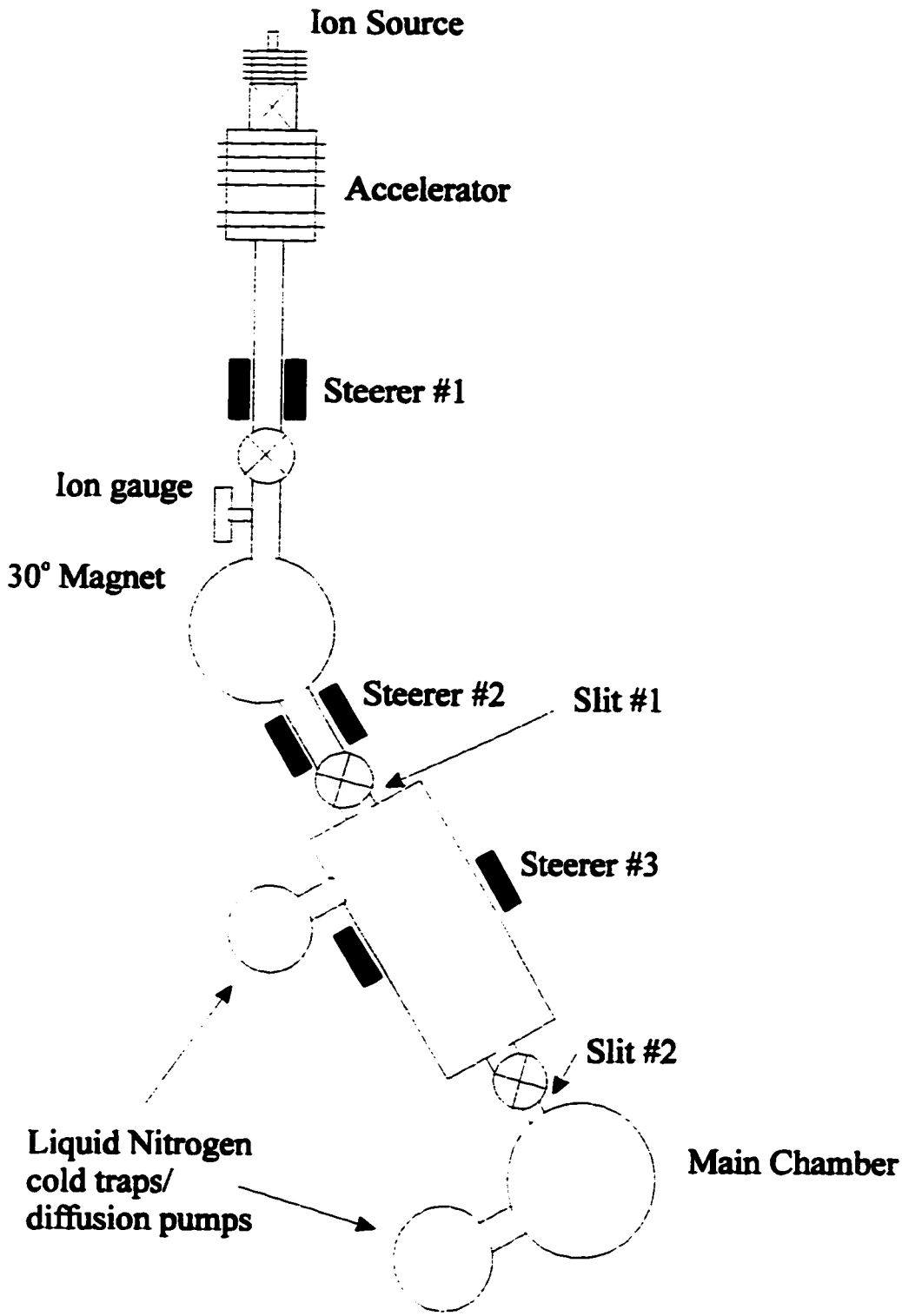

Figure 3.1 The experimental setup

This can be seen by taking into account the forces involved:

$$\frac{mv^2}{r} = qvB \tag{5}$$

where m is the ion mass, v is its velocity, q is its charge, r its radius of curvature and B is the magnetic field. One can express the velocity in terms of the accelerating potential V, $qV=mv^2/2$, which results in:

$$\frac{Vm}{q} = \frac{r^2B^2}{2}. \tag{6}$$

For this particular system, all particles that will pass through the complete apparatus will have the same radius of curvature. Hence, in equation (6), $r^2/2$ and V will be constant. If the magnetic field is varied, then different ions will pass through but the ion mass to charge ratio will all lie on the line when Vm is graphed as a function of I^2, see Figure 3.2.

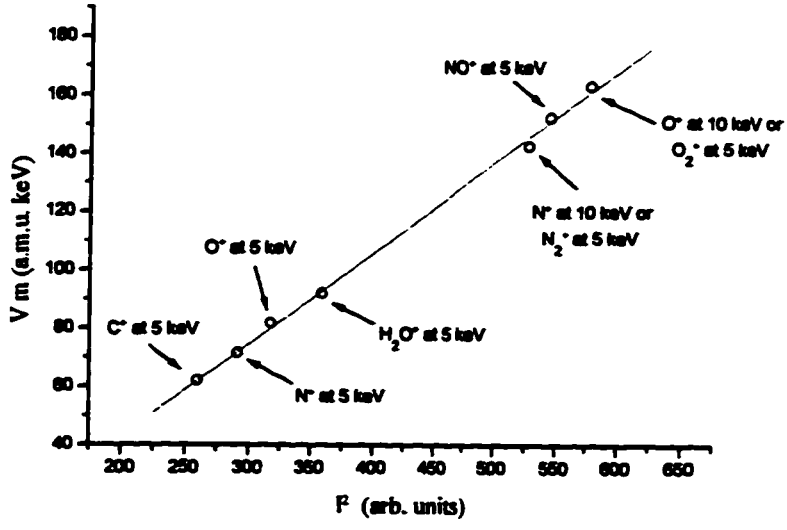

Figure 3. 2 Plot of I^2 vs. Vm

The points on the line in Figure 3.2 are actual experimental points taken from different mass scans at different accelerating potentials. The current, I, is proportional to the magnetic field produced by the magnet and therefore plotting Vm as a function of I^2 is nearly the same as plotting a function of B^2, ignoring hysteresis. All masses of all energies should thus lie on the same line and this calibration can then be used to identify other masses which come from the ion source.

3.1.2 Differential Section

The main purpose of this section is to separate the ordinary high vacuum of the accelerator, 10^{-6} Torr, from the UHV of the main chamber, 10^{-10} Torr, and to collimate the ion beam. This section normally operates at a pressure of about 10^{-9} to 10^{-8} Torr. The beam enters into the differential section through a slit that is 2 mm wide and 5 mm high. The exit slit, which is the entry point into the main chamber, is about 1.2m from the first slit and is about 0.25 mm wide and about 2 mm high. This exit slit has been made smaller in height by approximately 6 mm from previous work. This was done to insure better control of the placement of the ion beam on the target and to allow for a very tight beam with little angular dispersion from its initial trajectory. The final ion beam intensity on the sample was measured using an ammeter and was in the range a few nA.

The beam's direction could be adjusted effectively through the use of magnetic steerers. There are three along the beam trajectory between the accelerator and the main chamber: one just before the beam bending magnet; one just before the differential

section; and one half way along the differential section. A magnetic steerer produces adjustable transverse magnetic fields perpendicular to the direction of the beam. The steerers, which consist of four coils wound around an iron core placed around the beam but outside the vacuum, can make adjustments in both the vertical and horizontal directions. The coils that are opposite each other are connected in series which produce opposing fields inside the iron. The resulting magnetic field inside the vacuum is fairly uniform and stable and has an intensity of only a few hundred gauss, which is strong enough to deflect the ion beam by a few degrees but weak enough so that the iron is not saturated and the other possible adjustment is not affected. This results in two independent directional controls per steerer.

3.1.3 Main Chamber

The main chamber is illustrated in Figure 3.3. The sample is held in place by molybdenum clamps to a molybdenum sample holder, which is attached to the manipulator. This manipulator could be moved in the X, Y, and Z directions as well as rotation about the vertical axis and rotation about an axis normal to the plane of the surface. Measurements were taken in the horizontal (XY) plane. The angle involved with the vertical axis rotation is known as the elevation angle whereas the other rotation angle is referred to as the azimuthal angle. The three translational movements of the manipulator have a resolution of 0.005 mm. The elevation angle has a resolution of 0.1° whereas the azimuthal variation has a resolution of 0.3°. The two rotational movements

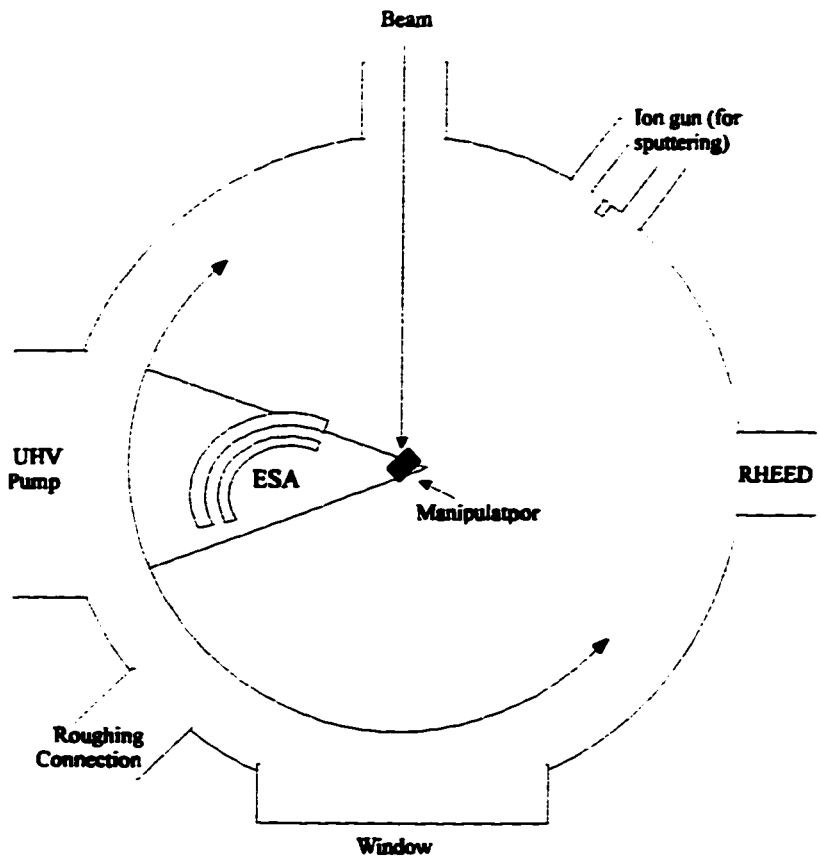

Figure 3.3 The main chamber.

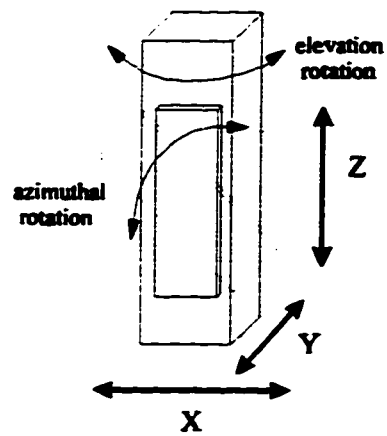

Figure 3.4 Illustration of possible movements of the manipulator.

allowed for different ways of testing the sample (this will be discussed later). For an illustration of these possible movements see Figure 3.4.

The manipulator was also equipped with an electron emission filament made out of thoriated tungsten located close to the back surface of the sample which allowed heating of the sample. A high negative voltage (250 V) was applied to this filament which resulted in up to a possible electron bombardment power of 25 Watts which allowed for heating to quite high temperatures up to about 1500K. The temperature produced was measured using a k-type chromel-alumel thermocouple attached to the sample holder very close to the sample. It was not attached to the sample itself to allow for easy removal/replacement of the sample and to avoid possible contamination of the surface.

The data was obtained using an electrostatic analyzer (ESA) which scans through the ion energy spectrum. One advantage of using an ESA as a spectrometer is that it can distinguish between multiply and singly charged ions. When using an ESA in order to obtain good statistics, data needs to be taken over as long a period of time as possible, from about a minute or so to half an hour or more. However, since the beam intensity is significant, several nA, the sample will be come damaged over these long periods of use. The strength of the beam and length of the run were optimized to obtain as good statistics as possible without significantly damaging the surface.

The present design of the ESA has been unchanged from previous work [2] but will be explained in detail here as it is an essential piece of equipment. The type of electrostatic analyzer that was used had a deflection angle of $\pi/\sqrt{2}$ (or 127°). It consists of

two cylindrically curved plates, separated by a small gap, with a slit at either end. In work by Hughes et al. [29], it was shown that ions which have approximately circular trajectories after passing through a deflection of $\pi/\sqrt{2}$, come to a first order focus. This type of focus is of limited use however since it lies inside the field region produced by the ESA. However, if the ions are deflected by an angle slightly less than $\pi/\sqrt{2}$ then the source and image points can be located in field free regions. The deflection angle was reduced to about 105° giving an image to field boundary distance of 5 mm when the object-field boundary distance was about 20 mm. The ESA was designed for a radius of curvature of 60 mm.

The main restrictions on the position of the analyzer were due to the range of motion required by the manipulator. The ESA, which was mounted on a moveable track to allow for a wide range of scattering angles, was placed far enough away from the manipulator so that at backward scattering measurements it would not block the beam. This distance is approximately 2 cm.

The energy resolution, to first order, can be expressed as

$$\frac{\Delta E}{E_o} = \frac{\Delta x}{R_o} \qquad (7)$$

where Δx is the image slit width and R_o is the central trajectory radius (or curvature radius of the central ray) [30]. For the particular ESA used $\Delta x \approx 1$ mm and $R_o \approx 60$ mm resulting in a resolution of 1 to 2% [2].

The particles that have passed through the ESA were counted by a channel electron multiplier (CEM) which was mounted behind the exit slit of the ESA. Another

CEM was mounted inside the main chamber. It was located close to the beam entrance slit and counted ions which had been scattered at ~180°. This second CEM was used to monitor any beam fluctuations and therefore could be used as a way to normalize the measurements, if deemed necessary. The front cones of the CEM's where biased with a negative voltage of 2 to 3 kV which repelled secondary electrons. Also, this second CEM could be used with a bias voltage of about +400V which was applied to an entrance aperture in front of the CEM. This removed low energy scattered positive ions. The data acquisition process will be explained in detail in section 4.1.

3.1.4 RHEED apparatus

Other measurements that could be done required the use of a reflection high energy electron diffraction apparatus (RHEED). This gave another way to obtain information about the surface crystallographic structure. The electrons produced by the RHEED strike the surface at sufficiently small angles as to only penetrate the first few

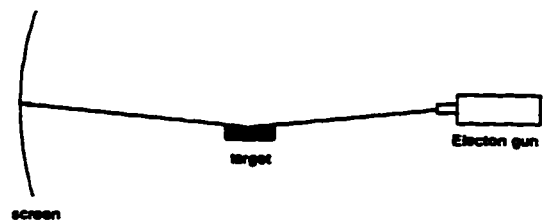

Figure 3.5 RHEED geometry.

atomic layers. These electrons produce a diffraction pattern, after striking the surface, on a fluorescent screen on the opposite side of the chamber from the electron gun, see Figure 3.5. This diffraction pattern can then be used to give rough estimates on the main dimensions of the surface unit cell and to determine the orientation of the sample.

3.1.5 Ion Beam Parameters

Several different elements can be used to create ion beams but in this work a positive oxygen ion beam was used. This particular type of beam was used primarily because it would not introduce a new substance to the surface and result in contamination. Another reason was that it would allow for easy distinction between peaks affected by the oxygen atoms and the titanium atoms on the surface.

The system, to obtain reasonable statistics, requires at least 1 nA. This intensity is easily obtained at higher energies but the ion extraction from the source was less efficient at lower energies and this set a lower energy limit at about 5 keV. As the intensity increases so does the damage to the surface. Therefore a beam intensity of 10 nA is too high. Typical intensities that were used are between 3 and 4 nA. This allowed for good statistics with minimal damage.

The possible range of energies that the beam can obtain are 5 to 150 keV. Typically values between 5 and 10 keV are used. The energy resolution, $\Delta E/E$, is of the order of 10^{-4}, which is negligibly small compared to its effect on measurements. The

angular spread of the beam is about 1 to 2 mrad. Both these values are determined from the geometry of the apparatus.

The energy resolution requirements on the beam were very critical which resulted in the beam being very sensitive to any adjustments in the deflection and steering magnets. This meant that all the equipment which could affect the beam's energy and or path had to be highly stable. For a steady beam, which did not drift during measurements all the power supplies had to be left on to stabilize for several days.

3.2 Experimental Preparation

3.2.1 Preparation of the Main Chamber

After the main chamber has been brought up to atmosphere, it needs to be properly cleaned before any measurements can be taken. To minimize contamination, nitrogen gas was let into the chamber and not air. Nitrogen limits the amount of water that attaches to the walls of the chamber and the equipment inside which, once there, is hard to remove. Once the system is isolated and pumped down to about 10^{-6} Torr range, the chamber needs to be baked, mainly to remove H_2O. A bake of about 12-14 hours with a maximum temperature of 473K was found to work well as this allowed time for the system to partially cool before degassing. Degassing is basically a heating process which causes impurities such as water and hydrocarbons to be transformed into their gaseous state and hence are removed from the chamber through pumping. After the bake, most equipment in the chamber was degassed, such as the heating element, the sputter gun, the electron gun for the RHEED apparatus, and the mass spectrometer. This was performed before the final cleaning of the sample.

3.2.2 Preparation of the Sample

Before mounting the sample in the UHV chamber it was cleaned using a chemical wash alternating between acetone and methanol. The sample was quickly air dried

between rinses to minimize film/residue on the surface. The sample was placed face-down in a prebaked crucible in order to reduce the amount of impurities from the walls of the oven that may deposit onto the surface. This crucible, with the sample, was placed in an oven and was baked to a temperature of 700°C and then cooled in air. This was an overnight procedure. It was thought that this prebake would limit the possibility of the sample fracturing in the chamber when heated as the heating rate was not always constant (there were fluctuations). After the sample was mounted, in the chamber and the system was baked, it was given a preliminary heating but only to a few hundred degrees. This heating degasses not only the heating element and the sample but the manipulator as well.

Before taking measurements the sample needed to be properly cleaned. After several successive sputtering and annealing as previously discussed in section 2.3, it was found that just annealing in oxygen was not sufficient to produce a smooth, impurity free surface. After the initial cleaning, the following process was found to provide a good, clean, stoichiometric surface. The first step is to sputter clean in a two step process. The first step is to sputter at 500V for 10-15 minutes in $5x10^{-6}$ Torr of argon (a current of $0.5\mu A/cm^2$ was measured). The second step is to sputter at 150V for five minutes at the same pressure at a current of $0.5\mu A/cm^2$. Since the best surface is one without steps or kinks and argon sputtering damages the surface and several layers down, it was decided that a change in the intensity of bombardment would reduce this subsurface damage. The results were good enough to suggest that this procedure was sufficient. A significant difference on the quality of the surface between a change in the energy of sputtering and no change at all cannot be stated here as this effect was not investigated. After sputtering,

the sample is then heated in a maximum of 10^{-6} Torr of oxygen for two minutes to 850-950K. This prevents oxygen vacancies on the surface and was also found to reduce the impurity level. As the oxygen was pumped away the sample was allowed to cool to about 500K or so. Next, the sample was annealed in UHV ($<10^{-9}$ Torr) for two minutes to 850-950K. From distinct RHEED patterns it was seen that this procedure seemed to produce a stoichiometric surface and removed any further surface impurities.

It was found that after several successive runs the surface was sufficiently damaged to give poor results. This damage included stoichiometric damage such as vacancies on the surface and the introduction of steps, kinks or holes and also the introduction of some impurities on the surface. Stoichiometric damage was determined by less intense peaks in the scattered ion energy spectrum where as impurities would introduce new peaks. It was decided that the cleaning process would be followed after each run so that the optimum surface conditions would be present for all measurements.

It was found that overnight exposure to pressures around $5x10^{-9}$ Torr or higher, did not result in the introduction of too many surface impurities, see Figure 3.6. Even exposure to pressures around 10^{-6} Torr for several days resulted in only a few impurities which could be removed after a few cycles of argon sputtering and annealing in oxygen, see Figure 3.7. The data shown in the two graphs shown in Figure 3.7 were taken shortly after a new sample was placed in the system so the initial cleaning processes were not yet completed. The data shown in Figure 3.6 were taken after this initial sputtering and annealing was completed and, as it can be seen, the result is a much cleaner surface. The

main reason for sputtering and cleaning the sample is, therefore, due to the damage of the surface by the ion beam and not the introduction of impurities. For a detailed interpretation of the spectra shown in Figures 3.6 and 3.7 refer to Chapter 4.

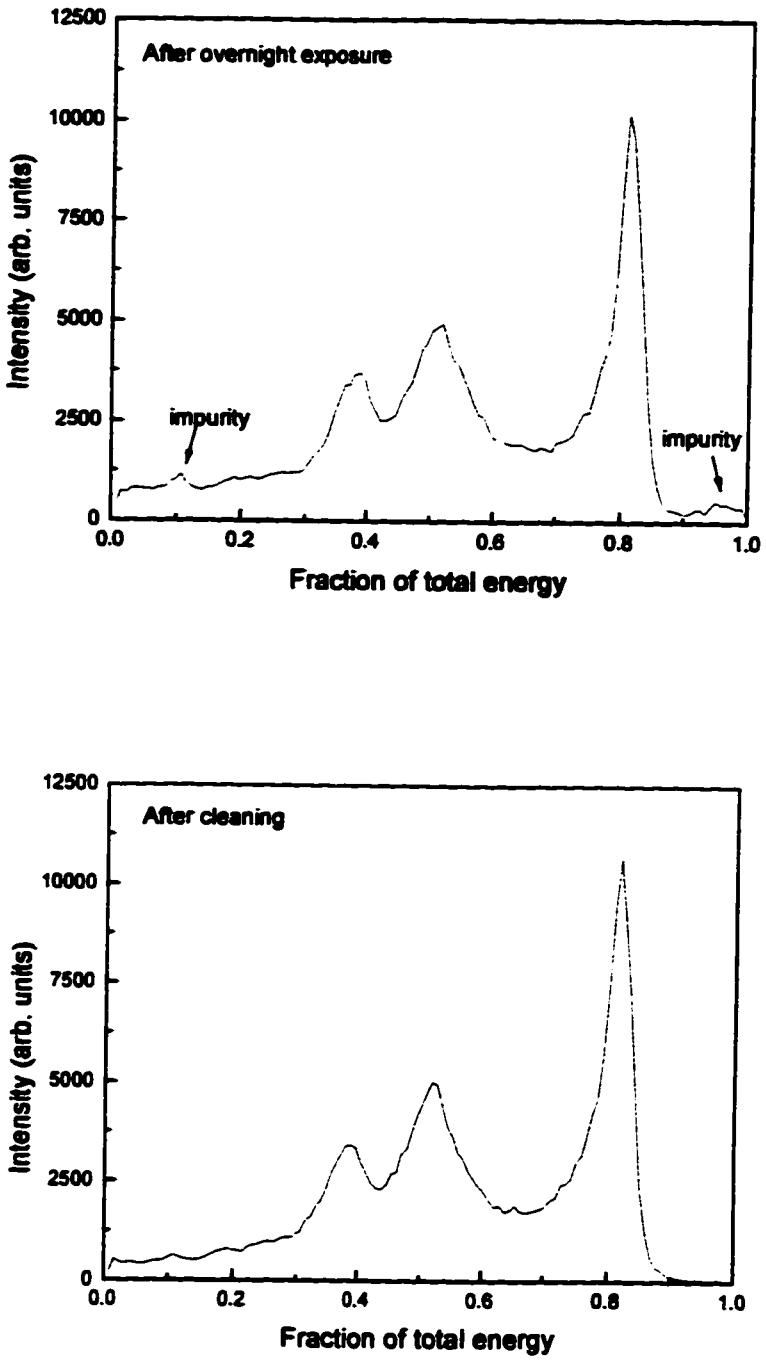

Figure 3. 6 Data shown here was taken with an angle of incidence (or elevation) of 5 and a scattering angle of 45°.

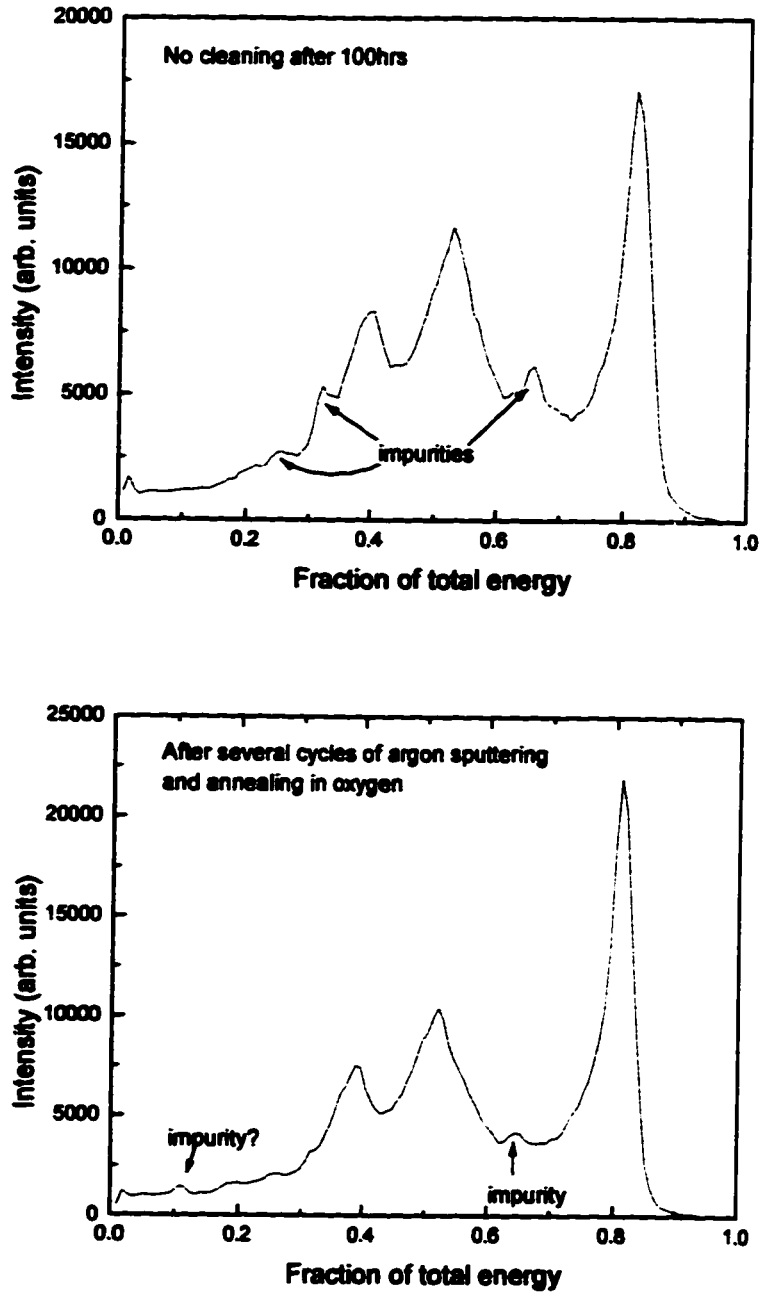

Figure 3. 7 Data shown here was taken with an angle of incidence (or elevation) of 5° and a scattering angle of 45°.

Chapter 4 Results and Discussion

4.1 Data Acquisition

Two sets of data are obtained for every run performed. The more important set of data is obtained through the ESA; this is where the information about the surface is found. The other set of data is obtained through a CEM at a deflection angle of ~180°, see section 3.1.4. This is used as a beam stability check and normalizer and is referred to as the monitor count.

The ESA is stepped through a specified number of channels and hence a specified voltage range. The voltages are supplied through programmable power supplies which are driven by a computer. The ESA voltage starts at zero voltage, the CEM will then count low energy ions for a specified length of time which is stored in an array. The voltage is then stepped up by a specified amount to count at a slightly higher energy and the process continues until the maximum channel is reached. Once this maximum is reached, the process is repeated again as the voltage is stepped down. The counts obtained with the same voltage are averaged. The data from the monitor is obtained simultaneously and stored in the same way.

The program used to obtain the data not only gives the choice of the range of voltages but also allows the choice of starting and ending channels, the length of time spent in each channel, and the number of times this process should be followed. If the last

parameter is chosen to be greater than one, the data is averaged after all the data has been obtained.

A variation on the program was needed to analyze a part of the energy spectrum for different settings of the geometrical parameters. The system, instead of averaging all the data over a specified range of values, stored each set of data separately. This process continued until the specified number of ranges had been achieved. A pause was introduced between each scan to allow time to manually make changes to the geometry. This procedure was used to obtain the variation of the ion yields as a function of the azimuthal angle or elevation angle.

There are some limitations when the length of time per channel is considered. If the time is too short the statistics will not be high enough to eliminate the affects any slight variation, i.e. noise, may have. Also, the ESA will not have sufficient time to stabilize at its new voltage before data is taken; this is the main limiting factor. If the time is too long, the sample will become damaged through long exposure to the beam and the surface may change dramatically over the course of one run. It was found that times of about 0.5 sec/channel were sufficient.

4.2 Energy Spectra

To obtain a spectrum the number of counts per channel are plotted vs. the channel number or fraction of the total energy. An example of a typical spectrum can be seen in Figure 4.1. The peaks correspond to single scattered ion-atom collisions. In the case of

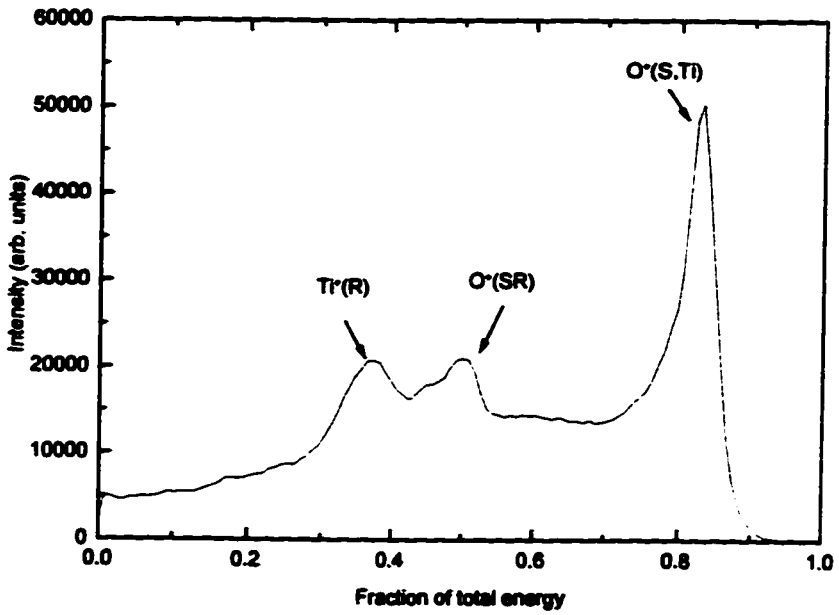

Figure 4. 1 A typical energy spectrum with θ=45° and θ_{in}=4°

TiO_2 there will usually be three main peaks: one due to oxygen scattered from titanium, denoted $O^+(S, Ti)$; another due to titanium recoil, $Ti^+(R)$; and oxygen scattered from oxygen and oxygen recoil, $O^+(SR)$. The last two possibilities are stated together since their energies are the same and will hence lie on top of one another. If another beam other than O^+, had been used, the energies may have been sufficiently different as to produce

separate peaks for the oxygen ions scattered from oxygen and the oxygen recoil ions. To obtain an estimation of the amount of ions scattered by titanium, for instance, the area of that particular peak is calculated. This will allow comparisons of the amount of ions scattered by Ti from one elevation angle or crystallographic direction to the next.

At certain scattering, azimuthal or elevation angles some peaks may not be present or may overlap with one another. Because of these possibilities, several scattering angles were investigated to see which ones would give the best results. The elevation and azimuthal angles were varied to investigate the surface, these results will be discussed later in this chapter.

This setup allows spectra to be taken at a range of scattering angles and energies. A few of the possibilities are shown in Figure 4.2. The scattering angles are 45°, 57°, 63°, 68°, 75°, and 77°. It can be seen easily that at different angles, some peaks are easily distinguishable from others, but other peaks lie on top of one another. For example at the higher scattering angles, the Ti^{+}(R) and the O^{+}(SR) peaks are indistinguishable. To see how the experimental positions of the peaks and the positions predicted by theory compare, refer to Table 4.1.

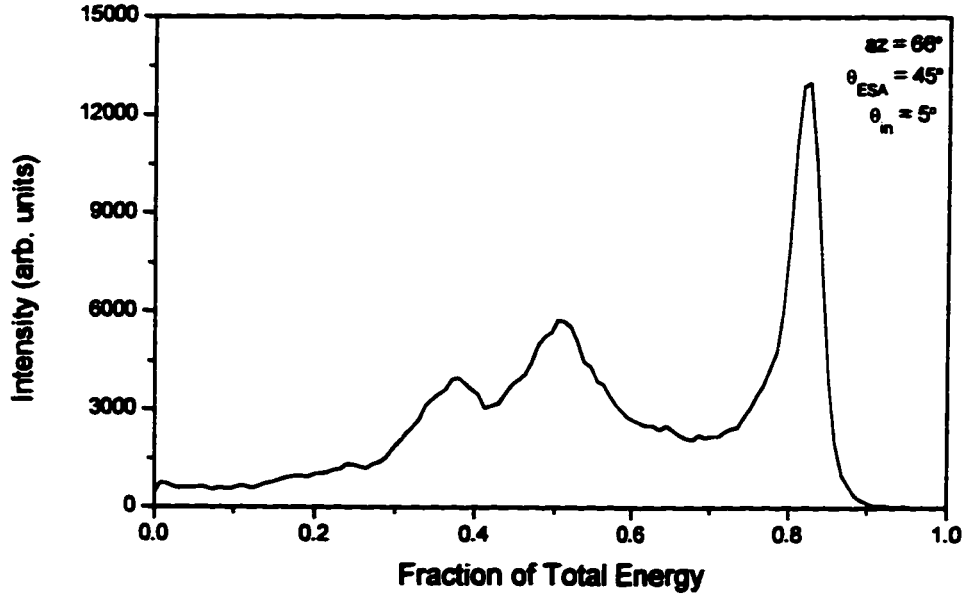

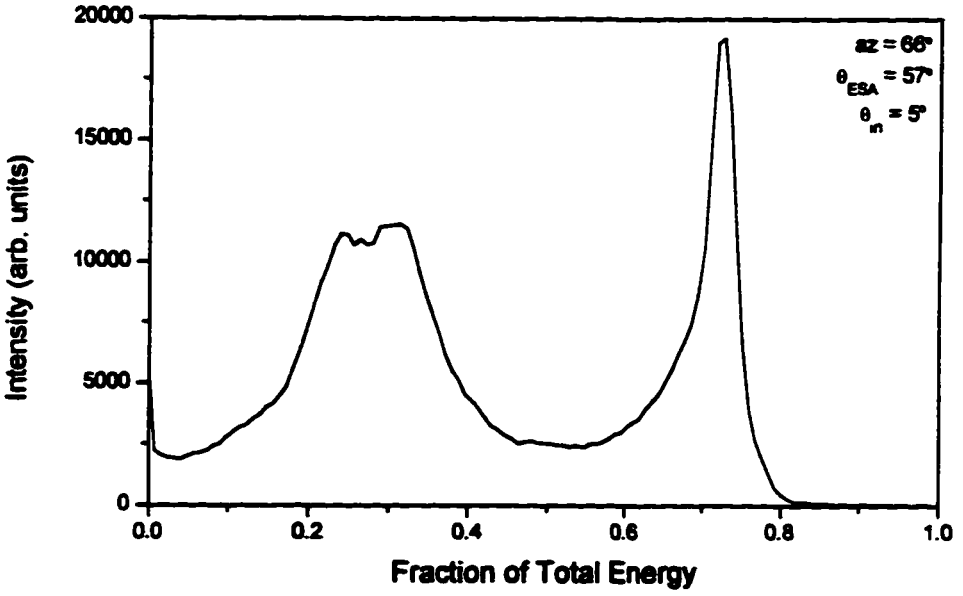

Figure 4.2a Data taken at an elevation angle of 5° and different scattering angles

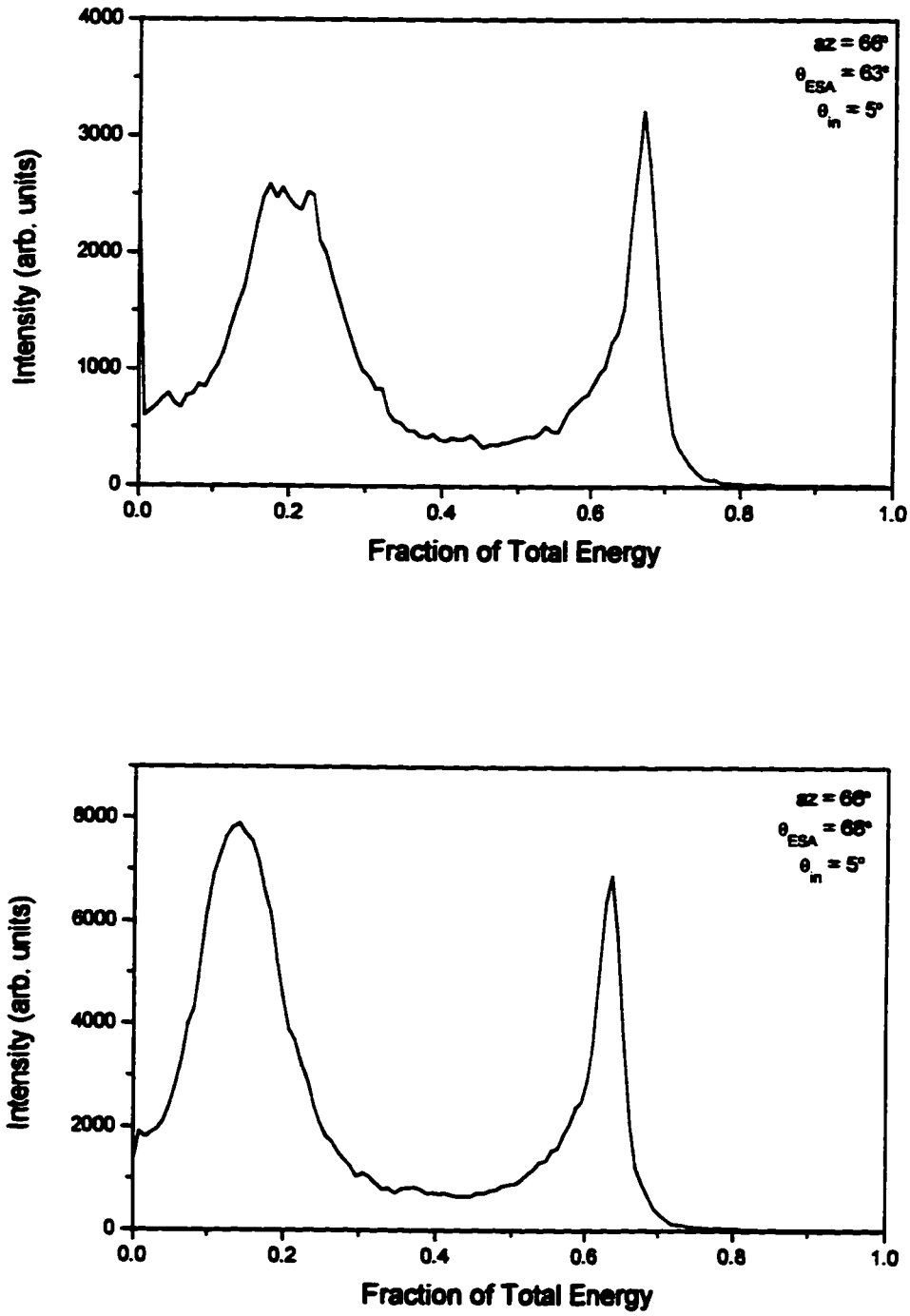

Figure 4.2b Data taken at an elevation angle of 5° and different scattering angles

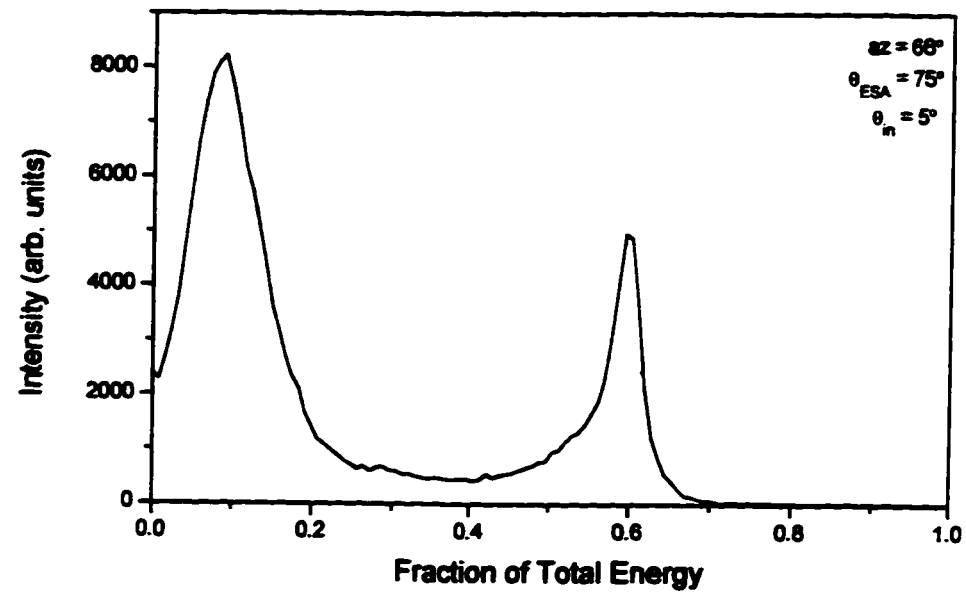

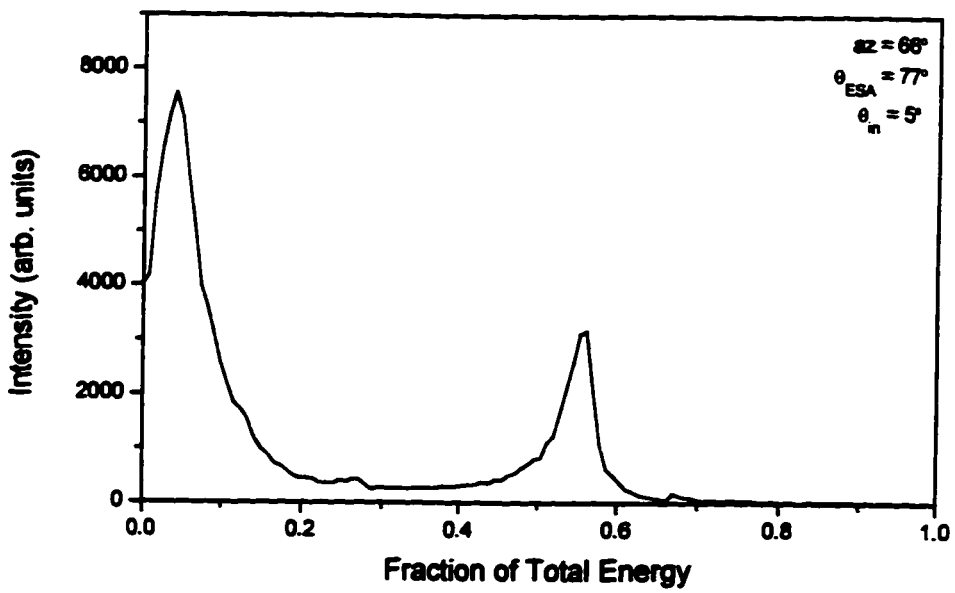

Figure 4.2c Data taken at an elevation angle of 5° and different scattering angles

Scattering Angle	O(SR) theory	O(SR) exp.	Ti(R) theory	Ti(R) exp.	O(S, Ti) theory	O(S, Ti) exp.
45°	0.50	0.50	0.38	0.38	0.82	0.82
57°	0.30	0.31	0.22	0.24	0.73	0.73
63°	0.21	.21/.23	0.15	.17/.18	0.69	0.67
68°	0.14	0.14	0.11	0.14	0.65	0.64
75°	0.07	0.09	0.05	0.09	0.60	0.60
77°	0.05	0.04	0.04	0.04	0.59	0.56

Table 4.1 Comparison of predicted and experimental positions of the peaks

It can be seen that at certain angles agreement between theory and experiment are quite good such as for $\theta = 45°$. In general the oxygen scattered from titanium peak has good agreement between theory and experiment with differences usually under 3% though sometimes a little higher. However, as the scattering angle is increased the agreement between theory and experiment for the other two peaks decreases quite dramatically, sometimes with a difference of 30% or more. This is mainly because the two peaks are sufficiently close that they appear as one peak and are given the same peak position which is not valid. This suggests that at these higher angles, the $Ti^{+}(R)$ and the $O^{+}(SR)$ peaks should not be used to obtain information about the surface or at least that any information that is obtained should be considered as a very rough estimate and possibly quite inaccurate.

4.3 Presence of Multiple Scattering

During an investigation of the surface cleaning procedures, it was noticed that a very broad peak was obtained, see Figure 4.3. At first it was thought that this peak was due to impurities with atomic masses in the region of 19 to 25 to produce scattered ions in this region. Earlier runs did not show this peak, refer back to Figure 4.2. However upon analysis, it was found that this peak was due to double and maybe even multiple scattering of the oxygen ions by oxygen atoms. This can be seen easily when one considers the values of k_s the exiting ion would have. Some possible values of k_s can be found in Table 4.2.

θ_1	θ_2	k_s
6	39	0.598
8	37	0.625
10	35	0.651
12	33	0.672
14	31	0.692
16	29	0.707
18	27	0.718
20	25	0.726
22	23	0.729
24	21	0.728
45	0	0.500

Table 4.2 Energy of double scattered oxygen ions with a total deflection angle of 45°

It can be seen that this peak appeared very noticeably when the beam was scattered in the $(\bar{1}10)$ scattering plane but not in the (001) scattering plane though in some instances it was still present. This suggests that the above surface oxygen rows,

which lie in the <001> direction, may have an effect on this multiple scattered peak. This multiple scattered oxygen peak is not always present for all elevations. The dependence of the presence of this peak on the elevation angle can give information of the shadow cone angles and the relative positions of atoms on the surface.

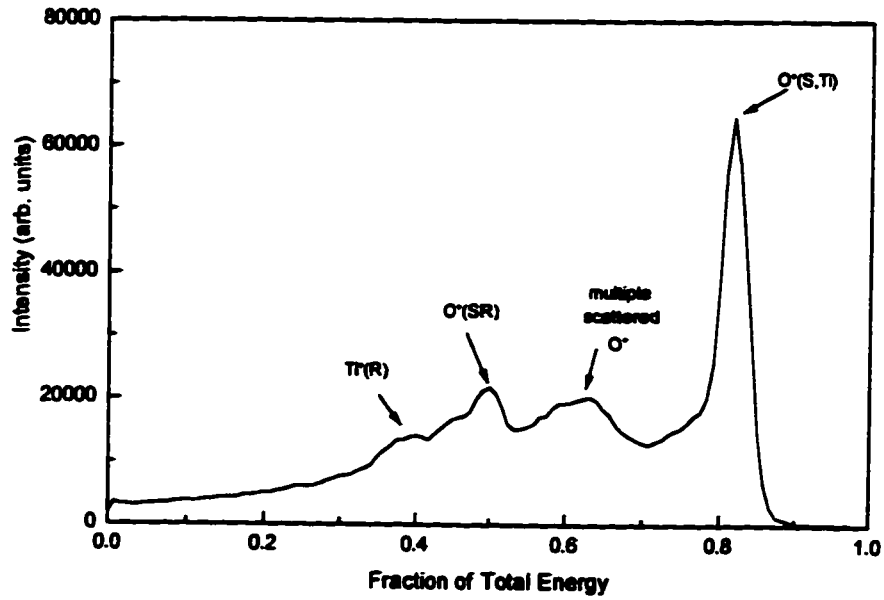

Figure 4.3 A typical energy spectrum showing the multiple scattered oxygen peak with $\theta = 45°$ and $\theta_{in} = 4°$

4.4 Azimuthal Scans[1]

An azimuthal scan varies the crystallographic direction that the ion beam strikes the sample while the elevation angle remains constant. To obtain as much information as possible without damaging the surface only one peak in the energy spectrum of the scattered ions and not the whole spectrum was measured. These scans would be repeated at different elevation angles. An example of these scans can be found in Figure 4.4. These scans have been symmetrized by taking the average area of the peaks at $\pm$ the azimuthal anlge, around the $<\bar{1}10>$ direction. The statistical errors are not shown. The minima in this plot correspond to one or more atoms being shadowed by the atom in front of it. These minima should occur along crystallographic directions where shadowing is most prevalent. Their positions agree well with the geometry of the (110) surface.

It can also be seen that the plots for oxygen and titanium are different; the peaks and valleys appear and disappear at different elevations. This is most likely due to the fact that titanium and oxygen occupy non-equivalent sites and therefore are shadowed by different atoms at different azimuthal angles.

Besides giving information on the orientation of the surface and possible shadowing relations, azimuthal scans can be used to give an estimate of shadow cone angles. The elevation and azimuthal angle positions of the steepest increases and decrease were plotted. These correspond to the shadow cone edges and should form a circle on a

[1] The data presented here and in section 4.5 have been previously reported in an article that will be published in the proceedings of the 5th International Conference on the Structure of Surfaces, in an edition of Surface Review and Letters (1996), but the results have been analyzed further.

graph where the axes are the elevation and azimuthal incident ion directions. The radius of this circle is an estimate of the shadow cone angle in that particular direction.

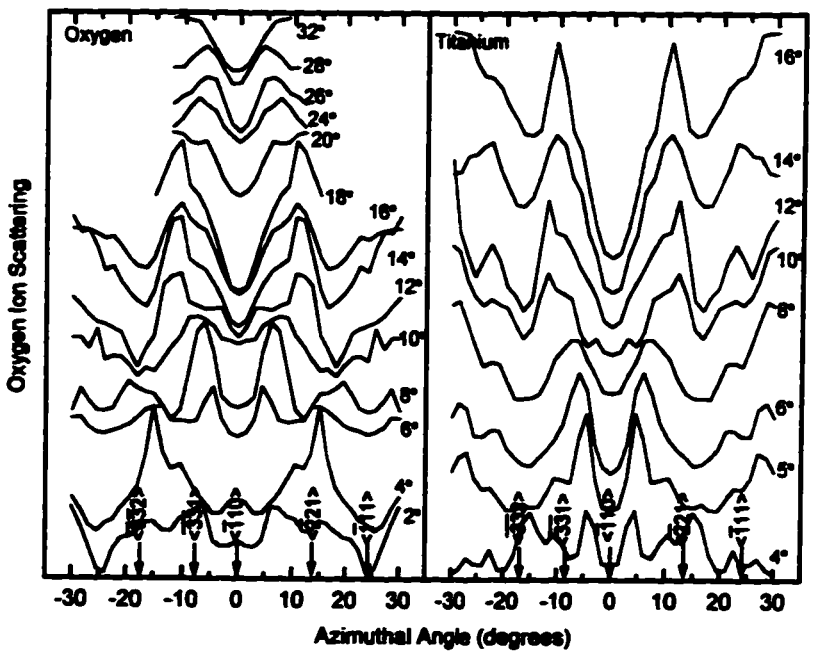

Figure 4.4 Azimuthal scans of both the oxygen scattered peaks; from oxygen atoms is on the left and from titanium is on the right. The scattering angle is $\theta = 5°$ and the angle adjacent to each curve gives the elevation angle θ_{in}

The data that has been obtained was used to construct such a plot, see Figure 4.5. Possible circles have been drawn. The fact that all the circle centers lie above an elevation angle of 0° suggests that the shadowing atom is higher than the atom involved in the scattering process. This shadowing atom could be an oxygen row atom which is above the surface or the atom that is shadowed is below the main surface plane.

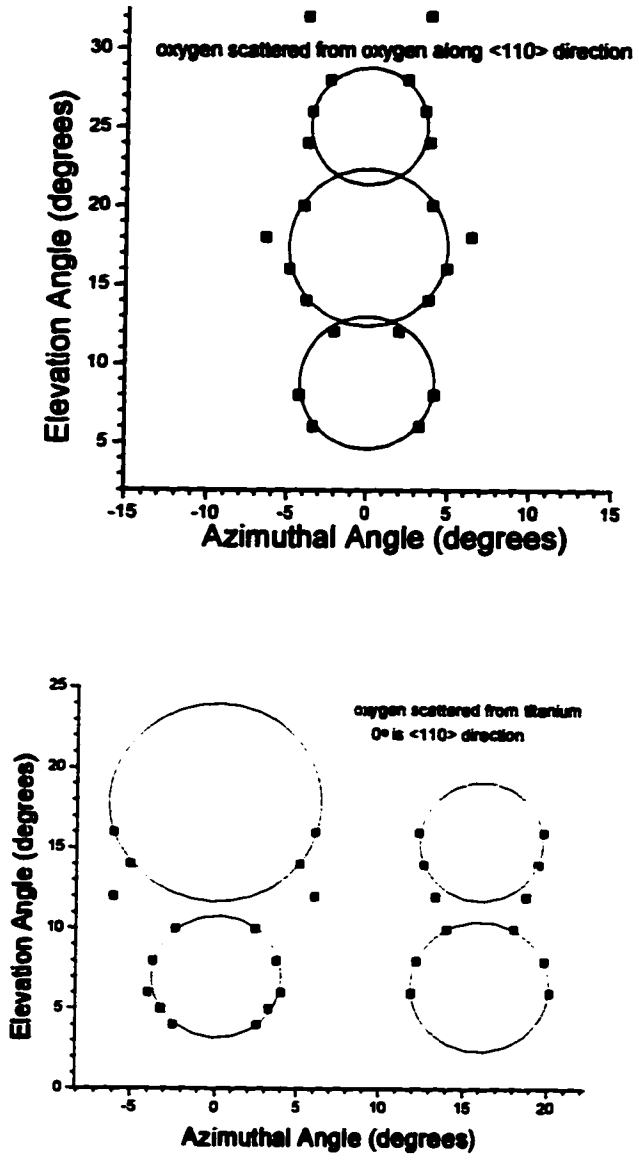

Figure 4.5 Circle plots for the data shown in Figure 4.4. Oxygen is on the top and titanium is on the bottom. The zero direction is perpendicular to the oxygen rows, the $<\bar{1}10>$ direction

The values of the diameters for the oxygen scattered from oxygen along the $<\bar{1}10>$ direction are 8.4°, 10°, and 7.2° located at elevations of 8.9°, 17.2° and 25.3°, respectively. The circle located at 8.9° corresponds to a surface titanium atom shadowing an oxygen atom that lies 3.245 Å (half the unit cell length in the $<\bar{1}10>$ direction) below the surface at a distance of 21.00 Å away from the titanium. For two atoms at this distance the corresponding shadow cone radius is 3.4° which agrees roughly with the experimental value of 4.2°. The circle located at 17.2° corresponds to an oxygen atom being shadowed by an oxygen row atom. The distance between these two atoms is approximately 10.2 Å but this value can vary depending on the height of the oxygen rows. If it is assumed that the oxygen rows are at a height that is the same as the bulk value, 1.285 Å, then the shadow cone radius is 4.9° which agrees well with the experimental value of 5.0°. However, the elevation angle would be 18.4°. If the oxygen rows are at a height lower than the bulk value, this elevation angle would be less. To have an elevation angle of 17.2° the height of the oxygen rows would be reduced to 1.05 Å resulting in a shadow cone angle of 5.0°. This suggests that the oxygen rows are significantly closer to the surface than the bulk value suggests. No corresponding relations between the atoms on the surface have been found to explain the third circle located at 25.3°. To have the correct elevation angle the resulting shadow cone radius is much greater than the experimental value of 3.6°. Likewise to have the correct shadow cone radius the resulting elevation angle would be lower than the experimental value. This may be a result of some surface atoms being displaced or steps or kinks that may be on the surface.

The diameters for the oxygen scattered from titanium for the $<\bar{1}10>$ direction are 7.8° and 12.3° at elevations of 7.0° and 17.8°, respectively. For the other direction at about 16° from the $<\bar{1}10>$ direction these diameters are 8.1° and 7.5° located at elevations of 6.6° and 15.4° respectively. The circle located at 7.0° in the $<\bar{1}10>$ direction is the result of an oxygen row shadowing a surface titanium at a distance along the surface of 9.73 Å. This suggests that rows of oxygen atoms may be missing, every second row, or that the incident ion is able to pass below these oxygen atoms. To have the proper elevation angle the oxygen row is at a height of 1.20 Å which is displaced from the bulk value of 1.285 Å. This elevation results in an atom separation of 9.81 Å which gives a shadow cone angle of 5° which corresponds roughly to the experimental value of 3.9°. Also in the $<\bar{1}10>$ direction, the circle located at 17.8° corresponds to a subsurface oxygen shadowing a subsurface titanium at a distance of 6.78 Å. This results in a shadow cone of 6.6° which corresponds reasonably well with the experimental value of 6.2°. The other shadowing direction is a result of two possible directions, $<\bar{2}21>$ and $<\bar{3}32>$ overlapping and this is the most probable explanation for any discrepancies between theory and experiment. The circle located at 6.6° corresponds roughly to an oxygen row atom shadowing a surface titanium along the $<\bar{3}32>$ direction. To have the correct elevation angle the oxygen row is at a height of 1.17 Å, which is, again, below the bulk value. This results in an atom separation of 10.2 Å and a shadow cone angle of 4.9° which compares well with the experimental value of 4.0°. The circle located at 15.4° does not have as good agreement with what is expected from theory. One possibility is that a subsurface titanium atom is shadowed by a surface titanium atom along the $<\bar{3}32>$

direction at an atom separation of 10.68 Å. This corresponds to an elevation of 17.6° and a shadow cone angle of 5.7°. Both of these values are too high, the corresponding experimental values are 15.4° and 3.8°. If the surface titanium atom is displaced by -0.4 Å then the elevation angle would be 15.6° but the shadow cone angle would still be about 5.7°. A displacement of such a large amount is also not very probable. This data suggests that shadowing in the $<\bar{3}32>$ accounts for the shadowing seen and shadowing in the $<\bar{2}21>$ direction has little effect on the results.

A summary of the results and an estimate of the errors involved can be found in Table 4.3, below. The errors shown in Table 4.3 have been determined by fitting other circles to the plots shown in Figure 4.5. These errors, however, may not be a true representation of the actual uncertainties. In fact the uncertainties are probably much higher than those stated here but it can be said that the height of the oxygen rows appears to be lower than the bulk predicted value.

Discrepancies may be accounted for the fact that it its assumed that most atoms lie on the same surface plane with no shifting above or below the surface. The results would be affected if the surface atoms are displaced. Also, the peaks that were analyzed to give the information on the oxygen scattered from oxygen also contains the oxygen recoil atoms which may affect the results though this effect would be small. There may also be steps on or kinks in the surface as well as missing atoms. Multiple shadowing by several atoms may also have an effect. Further data needs to be taken which may result in new circles or some circles being larger or smaller than have been drawn. The data does suggest that the oxygen rows are not at height of 1.285Å above the surface which is

surface which is suggested by the bulk but are in fact closer to the surface. The values found here range from 1.20Å to 1.05Å, a difference of -7% to -18% from the bulk value.

Oxygen scattered from oxygen:

Elevation angle, exp.	Elevation angle, exp.	Elevation angle,adjust.	Shadow cone, exp.	Shadow cone, theory	Shadow cone, adjust.	Est. oxygen height
8.9° ± 0.3°	8.9°	N/A	4.2° ± 0.1°	3.4°	N/A	N/A
17.2° ± 0.3°	18.4°	17.2°	5.0° ± 0.2°	4.9°	4.9°	1.05±0.05Å
25.3° ± 0.6°	??	N/A	3.6° ± 0.2°	??	N/A	N/A

Oxygen scattered from titanium

Elevation angle, exp.	Elevation angle, exp.	Elevation angle,adjust.	Shadow cone, exp.	Shadow cone, theory	Shadow cone, adjust.	Est. oxygen height
7.0° ± 0.3°	7.5°	7.0°	3.9° ± 0.1°	5.0°	5.0°	1.20±0.06Å
17.8° ± 0.6°	16.8°	N/A	6.2° ± 0.2°	6.6°	N/A	N/A
6.6° ± 0.3°	7.2°	6.6°	4.0° ± 0.2°	4.9°	4.9°	1.17±0.05Å
15.4° ± 0.6°	17.6°	N/A	3.8° ± 0.2°	5.7°	N/A	N/A

Table 4. 3 The results for the azimuthal scans. The theoretical values are obtained using the predicted bulk values. The adjusted values correspond to an adjustment of the height of the oxygen rows so that the elevation angles are in agreement.

Work done by Charlton, et al [25] has shown that the surface atoms, oxygen rows and even the second layer atoms are displaced from the predicted bulk values. Theory

done by Ramamoorthy et al [31] has predicted this to be the case. In this present work it was assumed that all the atoms except the oxygen rows were at their predicted bulk positions. This however does not seem to be the case and may be the major reason why there are discrepancies between the predicted and experimental shadow cone values.

If the displacements given by Charlton are considered when analyzing the data shown in Figure 4. , the results presented here do not differ greatly. The reason for this is most likely because the presented results see the difference between two atoms and not their displacements from their bulk predicted values. The differences between atoms agree roughly with the differences between atoms given by Charlton. The circles will still be explained by the same shadowing and the values of the shadow cones do not differ greatly. In fact the difference in the height of an oxygen row atom and a titanium surface atom correspond to the height of the oxygen rows found here. Charlton's value would be 1.175Å (found by taking the bulk value of 1.285 and subtracting the oxygen row contraction of 0.27 and adding the titanium atom displacement of 0.16) which falls into the range reported here, from 1.05Å to 1.20Å, not including errors.

However, if the same is performed with the results Ramamoorthy has produced the result is actually higher than the 1.285Å bulk value: 1.285-0.07+0.17=1.385Å. So when the displacement of the titanium surface atom is considered, the relative distance between it and the above surface oxygen is disagreed upon. Ramamoorthy shows that it is greater than the bulk value where Charlton and this work shows that it is lower.

4.5 Elevation Scans

Another way to obtain information about the structure of the (110) surface is to vary the ingoing angle to the surface of the ion beam θ_{in}. By using the multiple scattered oxygen peak, the radii of the shadow cones and hence the separation of the atoms can be estimated.

In Figure 4.6, the energy spectra are shown for different elevations and for the two main crystallographic directions. In Figure 4.6(a), the (001) scattering plane, there is a shift in energy between 6° and 8° degrees in a small peak between the oxygen scattered from oxygen and oxygen scattered from titanium peaks. This peak is interpreted as a double (or multiple) scattering process. This critical angle, as an estimate to the shadow angle, would correspond to an atom separation of 5.2 Å to 7.8 Å; resulting in an average of 7° and 6.5Å. The actual separation of the oxygen rows is 6.49 Å and the shadow cone angle is 7.1°. In the $(\bar{1}10)$ scattering plane, see Figure 4.6(b), this energy shift occurs between 12° and 14° which corresponds to a separation of 2.3 Å to 2.9 Å; resulting in an average of 13° and 2.6 Å. The actual separation of the atoms in the oxygen rows is 2.96 Å and the shadow cone angle is or 11.7°. The results and theory agree fairly well especially in the (001) scattering plane as the theoretical results are practically the same as the average experimental results. The results for the $(\bar{1}10)$ scattering plane, however, are lower than expected. This may be a result of surface atoms being displaced from the surface plane. Also, since these peaks involve multiple scattering, the shadowing process

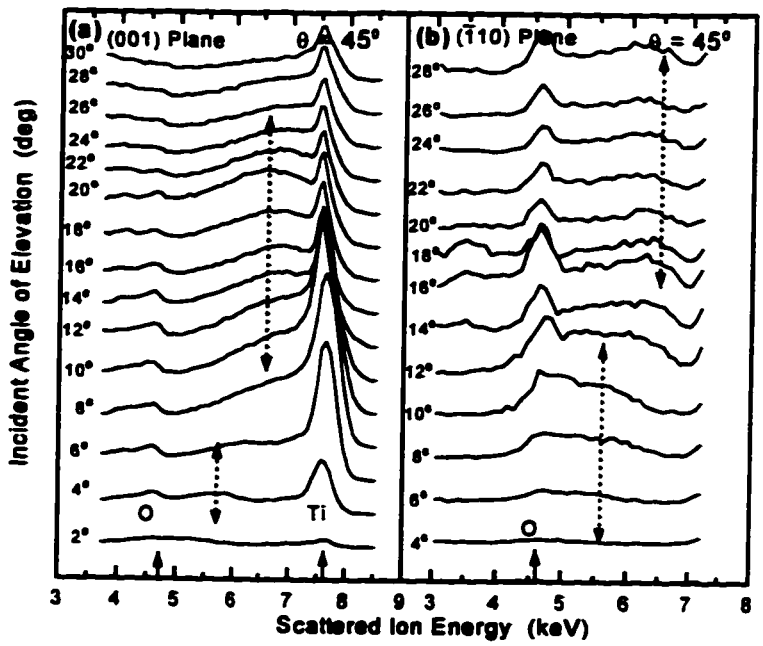

Figure 4.6 Elevation scans of the multiple scattered oxygen peak (marked with the dotted lines)

may be more complicated. There may also be steps or kinks in the surface which may cause the surface to appear contracted resulting in smaller atomic separations. Another possible reason is that this experiment cannot distinguish between recoiled and scattered oxygen ions/atoms. This is because the trajectories of a recoiled and scattered oxygen atom/ion are not the same even though their energies may be equal though this effect would be small.

One way to obtain an estimate of the height of the oxygen rows is to plot the peak area of titanium as a function of the elevation angle. The resulting curve will have 'dips' that correspond to shadowing of the titanium atoms by other atoms in the surface region. The easiest direction to perform this experiment is through the (001) scattering plane,

along the $<\bar{1}10>$ direction. The plot shown in Figure 4.7 shows several 'dips' in the curves, for the (001) scattering plane. The first few dips can be accounted for by atoms being shadowed by other atoms in the same plane. For example, the dip that occurs at about 7° is due to titanium shadowing other titanium atoms in the same plane at a separation of 6.49 Å which has a theoretical shadow cone of 7.1° or due to an oxygen atom shadowing a titanium atom at a separation of about 4.5 Å which has a shadow cone of 8.7°, also in the same plane. The difference of the shadow cone angles suggests that this dip is due mainly to titanium shadowing. It is possible that some of the dips that occur at higher angles are due to some subsurface scattering or due to the fact that some of the surface atoms may be displaced from the surface plane.

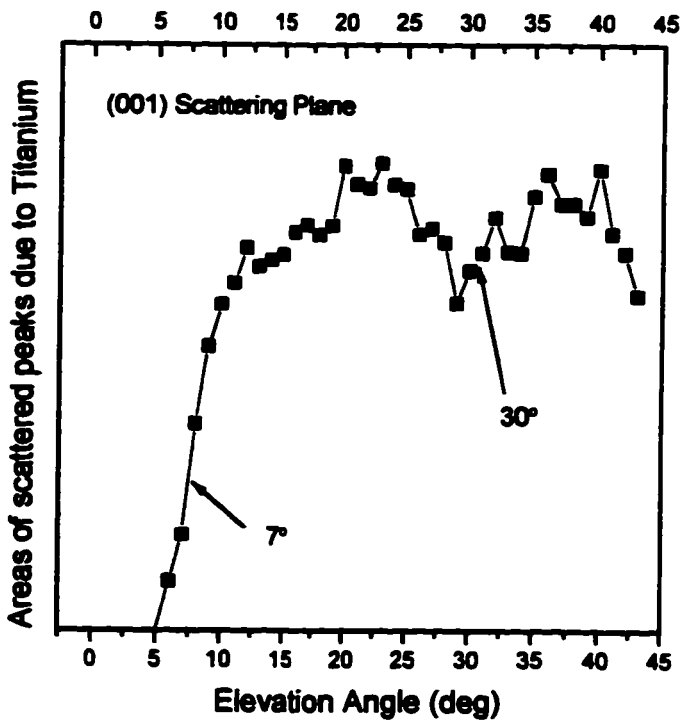

Figure 4.7 Elevation scans of oxygen from titanium in the (001) scattering plane.

The dip and rise occurring between 28° and 32° is due to the shadowing of titanium atoms by the oxygen rows. The halfway angle of 30° is equal to the shadow cone angle, α, and the elevation angle between the oxygen atom and the titanium atom, δ; i.e. $30° = \alpha + \delta$. First it was assumed that the oxygen rows are at a height above the surface that is much like the bulk value (1.285 Å). Using this value, and knowing the separation of the atoms, both α and δ can be determined. It was found that this height gave a too high value of $\alpha + \delta$. By lowering the value used for the height of the oxygen rows, the value of $\alpha + \delta$ was closer to the experimental value. The height of the oxygen rows that gave the closest value was 1.15 ± 0.05 Å. This value lies within the range determined in the previous section (section 4.4). This is a displacement of 0.135Å toward the surface plane, a 10% difference from the bulk which can be considered as a significant difference.

Chapter 5 Conclusions

From this work it has been shown that the experimental positions of the peaks in the emitted ion energy spectrum agree well with the predicted values for simple ion-atom scattering but with a fair amount of multiple scattering by oxygen atoms.

Shadow cone angles have also been estimated and are in good agreement to what theory suggests, for specifics refer to sections 4.4 and 4.5. The unit cell dimensions of the surface of TiO_2 correspond roughly to the dimensions of the bulk unit cell, 6.49 Å and 2.96 Å.

It was shown, both in the azimuthal and elevation scans, that a fair amount of the scattering was subsurface.

The height of the oxygen rows present on the surface has been found to be lower than the predicted bulk height of 1.285 Å. Depending on the experiment the height has been as high as 1.20 Å and as low as 1.05 Å for the azimuthal scans and 1.15 for the elevation scans. These values differ by about 15%. This suggests that the accuracy of these results are questionable and in fact the uncertainties of the results are probably higher as previously stated in section 4.4. The difference of 15% can be used as an estimate for the accuracy of the experiment. It can be said for certain that the height of the oxygen rows is lower than the bulk predicted value but as to the actual value further experimentation is required which would also improve the accuracy.

As always there are others things that could have been done or that should be done as a result of this work. Possible further experimentation should be done to discover

if the surface atoms lie within the same plane or if there is some shift above or below the surface as this will effect the result of the oxygen height above the surface plane. Also, it would be advantageous to obtain atomic distances of the other atoms in the surface unit cell other than just the corners of the cell. Further experimentation should also be performed to obtain a better measurement of the height of the oxygen rows. Such experiments would include the azimuthal and elevation scans being done over a larger range of angles and at smaller angle intervals. Also, these experiments should be performed on many samples.

Further experimentation has already been performed after this work was completed which has shown that multiple shadowing by several atoms may occur and hence the theory would be more complicated. This may account for discrepancies in the results and theory [32].

Another possible experiment is to repeat the measurements with a different ion beam, such as helium. It would be then possible to measure at backward scattering angles where there are no recoil ions. This would eliminate any problems with the overlap of oxygen scattered and recoil peaks as there would not be any scattered oxygen, only scattered helium. By performing the same experiments, it could be investigated if this overlap did have an affect on the results.

References

[1] B. Hird, R.A. Armstrong and P. Gauthier, *Physical Review B*, **48**(1993) 3654-; B. Hird, R.A. Armstrong and P. Gauthier, *Nuclear Instruments and Methods in Physics Research B*, **90** (1994) 243; B. Hird, R.A. Armstrong and P. Gauthier, *Surfacae Science*, **292** (1993), 305; B. Hird, P. Gauthier, J. Bulicz, and R.A. Armstrong, *Physical Review Letters*, **67** (1991) 3575; and B. Hird R.A. Armstrong, P. Gauthier and J.A. Seel, *Physical Review B*, to be published, accepted August 1996

[2] B.Hird, P.Gauthier and R.A.Armstrong, *Rev. Sci. Intsrum.*, **66** (1995) 3273

[3] B. Hird, R.A. Armstrong and J.A. Seel, to be published in the proceedings on the 5th International Conference on the Structure of Surfaces, 1996

[4] Y.W.Chung, W.J.Lo, and G.A.Somorjoi, *Surface Science*, **64** (1977) 588

[5] Victor E. Henrich, G. Dresselhaus and H.J. Zeiger, *Physical Review Letters*, **36** (1976) 1335

[6] R.H.Tait and R.V.Kasowski, *Physical Review* **B20** (1979) 5178

[7] Michael Sander and Thomas Engel, *Surface Science Letters*, **302** (1994) L263

[8] Andras Szabo and Thomas Engel, *Surface Science*, **329** (1995) 241

[9] B.L.Maschhoff, Jain-Mei Pan and Theodore E. Madey, *Surface Science*, **259** (1991) 190

[10] S.Thomas, *Surface Science*, **55** (1976) 754

[11] J.-M. Pan, B.L. Maschoff, U. Diebold, and T.E. Madey, *Journal of Vacuum Science and Technology A*, **10** (1992) 2470

[12] R. Souda et al *Surface Science*, **285** (1993) 265

[13] S.R. Kasi, H. Kang, C.S. Sass and J.W. Rabalais, *Surface Science Reports*, **10** (1989) 1

[14] David P. Smith, *Journal of Applied Physics*, **38** (1967) 340

[15] Goldstein, Classical Mechanics (1981) Addison Wesley Publishing Co., Inc (USA), 2nd edition

[16] Chr. Lehmann and G. Leibfried, *Zeitschrift für Physik*, **172** (1963) 465

[17] Edgar Everhart, Gerald Stone and R.J. Carbone, *Physical Review*, **99** (1955), 1287

[18] E. Gofuku, Y. Toyoda, Y. Uehara, M. Kohara and M. Nunoshita, *Applied Surface Science*, **48/49** (1991) 343

[19] Richard L. Kurtz, *Surface Science*, **177** (1986) 526

[20] L. Wang, J. Liu, J.M. Cowley, *Surface Science*, **302** (1994) 141

[21] C.C. Kao, S.C. Tsai, Y.W. Chung and W.J. Lo, *Surface Science*, **95** (1980) 1

[22] B. Grossman and P. Piercy, *Physical Review Letters*, **74** (1995) 4487

[23] Preben J. Møller and Ming-Cheng Wu, *Surface Science*, **224** (1989)

[24] Hiroshi Onishi, Yasuhiro Iwasawa, *Surface Science*, **313** (1994) L783

[25] G. Charlton et al, to be published in the proceedings on the 5th International Conference on the Structure of Surfaces, 1996

[26] Göpel, J.A. Andrew, D. Frankel, M. Jaehing, K.Phillips, J.A. Schäfer and G. Rocker, *Surface Science*, **139** (1984) 333

[27] Bardi, K. Tamura, M. Owari and Y. Nihei, *Surface Science*, **32** (1988) 352

[28] Master of Science thesis, 1992, Pierre Gauthier, University of Ottawa

[29] A. L. Hughes and V. Rojansky, *Physical Review*, **34** (1929) 284

[30] W. Steckelmacher, *Journal of Physics E: Scientific Instruments*, **6** (1973) 1061

[31] Madhavan Ramamoorthy and David Vanderbilt, *Physical Review B*, **49** (1994), 16721

[32] Private communication with B. Hird